Modeling of Moisture Diffusion in Permeable Fiber-Reinforced Polymer Composites Using Heterogeneous Hybrid Moisture Element Method

De-Shin Liu[1], Zhen-Wei Zhuang[1], Shaw-Ruey Lyu[2,3]
Cho-Liang Chung[4] and Pai-Chen Lin[1]

Abstract: This study proposes a two-dimensional heterogeneous hybrid moisture element method (HHMEM) for modeling transient moisture diffusion in permeable fiber-reinforced polymer composites.

The HHMEM scheme is based on a heterogeneous hybrid moisture element (HHME), with properties determined through an equivalent hybrid moisture capacitance/conductance matrix. This matrix was calculated using the conventional finite element formulation in space discretization as well as the θ-method in time discretization with similar mass/stiffness properties and matrix condensing operations. A coupled HHME-FE scheme was developed and implemented in computer code *MATLAB* in order to analyze the transient moisture diffusion characteristics of composite materials containing multiple permeable fibers. The analysis commenced by comparing the performance of the proposed scheme with that of conventional FEM to model the moisture diffusion process. Both hexagonal and square fiber arrangements were studied. Having validated its performance, the scheme was then employed to investigate the relationship between the volume fraction of the permeable fibers in the resin composite and the rate of moisture diffusion. It was found that the moisture diffusion was significantly retarded as the volume fraction of the fibers increased.

The HHMEM approach proposed in this study provides a straightforward and efficient means of modeling transient moisture diffusion in composite materials containing multiple permeable fibers. This is because only one HHME moisture char-

---

[1] Advanced Institute of Manufacturing for High-tech Innovations and Department of Mechanical Engineering, National Chung Cheng University, 168, University Rd., Min-Hsiung, Chia-Yi, 621, Taiwan, R.O.C.

[2] Corresponding author. Tel.: +886-5-2648000 (Ext: 5901); fax.: +886-5-2648000 E-mail address: srlyu@ms5.hinet.net

[3] The Joint Center, Tzu Chi General Hospital, Chia-yi, 621, Taiwan, R.O.C.

[4] Department of Materials Science and Engineering, I-Shou University, No. 1, section 1, Shiuecheng Road, Dashu Shiang, Kaohsiung Country, Taiwan, 840, R.O.C.

acteristic matrix of fibers requires calculation for all HHMEs sharing the same characteristics. Furthermore, varying volume fractions can be modeled without modifying the original model simply by controlling the size of the inter-phase region within the HHME domain.

Keywords: Modeling multiple permeable fibers, Transient moisture diffusion, Heterogeneous hybrid moisture element method.

1   Introduction

Fiber-reinforced polymer composites absorb moisture during their service life, principally through their resin matrix, as well as through their fibers when they are permeable [Tsai and Hahn (1980)]. The moisture impacts the mechanical properties of composites, binding capacities and interfaces. Because of these effects, it is of interest to determine how quickly moisture will diffuse into the composite.

The moisture diffusion characteristics of composites have attracted considerable attention [Shen and Springer (1977); Browning, Husman and Whitney (1977)]. Typically, transient moisture diffusion under normal environmental conditions is approximated as a Fickian process. Thus, the analytical models designed to explore the moisture diffusion characteristics are drawn from a homogenized model. In homogeneous materials, the transport of moisture is governed by (1) the maximum moisture content (which generally varies as a strong function of the relative humidity) and (2) the effective diffusivity (which typically varies as a strong function of temperature and the volume fraction of the fibers). However, the effective or average properties ignore the micro-structural heterogeneity. Hence, the homogenized rule-of-mixtures approach may not effectively describe the time-dependent moisture content field under transient conditions [Vaddadi, Nakamura and Singh (2003)].

Researchers have expended an enormous amount of effort on developing various numerical techniques for modeling and calculating heterogeneous materials with imbedded inclusions and surrounding interphase. A numerical model, called representative volume element (RVE), was proposed to represent unidirectional fiber-reinforced composites. Several studies [Yang, Yang, Ma and Liu (2010); Gueribiz, Rahmani, Jacquemin, Frèour, Guillèn and Loucif (2009)] exist in which the RVE was analyzed to determine the effective moisture diffusivity of composite material. The RVE was chosen as the basic cell of the composite medium. However, some issues need to be carefully addressed when carrying out such analyses. First, the correct RVE corresponding to the assumed fiber distribution must be isolated. Second, the correct boundary conditions must be applied to the chosen RVE in order to model the various load situations.

The conventional finite element method (FEM) is commonly employed in such situations as it provides a convenient means of understanding the mechanical behaviors of fiber-reinforced composites [e.g., Aditya and Sinha (1996); Vaddadi, Nakamura and Singh (2003); Pahr and Böhm (2008); Takashima, Nakagaki and Miyazaki (2007)]. However, a large number of fine finite elements are required, and mesh modeling is generally a tedious and complicated task, particularly when the aim is to clarify the relationship between the volume fraction of the fibers and the specific property of the materials.

In a series of related studies, Liu and Chiou (2003-2005) discussed the recent developments in 2-D and 3-D infinite element methods (IEM). The conventional IEM approach was implemented through computer codes to deal with the various types of classical elasticity and singularity problems. Liu, Chiou and Chen (2004-2005) also extended the IEM to address elastostatic problems in which the constituent material properties were heterogeneous. The related background and knowledge of the earlier work is summarized in the literature [Guo (1979); Ying (1995)]. However, to date, IEM analysis has been limited to the solution of solid mechanics problems.

This study develops a novel, efficient and convenient numerical technique, known as the heterogeneous hybrid moisture element method (HHMEM), to characterize transient moisture diffusion in composite materials with permeable fibers. Both hexagonal and square fiber arrays are considered in the matrix. The proposed numerical method is used to study the transient moisture diffusion process; this includes the effects brought about by varying the volume fraction on the rate of moisture diffusion.

2   Heterogeneous hybrid moisture element method

In this section, a heterogeneous hybrid moisture element formulation is derived for modeling the 2-D transient moisture diffusion problem. The basis of the proposed method is a heterogeneous hybrid moisture element (HHME) in which exists an elastic inclusion or a void of arbitrary geometry (for example, circle), as shown in Fig. 1(a). The element domain is decomposed into two separate sub-domains, as shown in Fig. 1(b) and (c), each with dissimilar material characteristics. The two domains represent, respectively: (I) the inter-phase sub-domain with boundaries Γ_0 and Γ_s; and (II) the inclusion sub-domain with a boundary Γ_s. Γ_0 and Γ_s comprise, respectively, the element's outer boundary accompanied by neighboring elements as well as the inner interface boundary between the inter-phase and the inclusion sub-domains. The derivations below initiate by establishing the element matrix equation.

2.1 Governing equation of moisture diffusion

In the existing modeling method, the transient moisture diffusion equation is analogous to that of heat conduction. The analogous technique for a homogeneous material system [Crank and Park (1956)] has recently been extended to include a multi-material system [Wong, Teo and Lim (1998); Wong, Rajoo, Koh and Lim (2002)], and hence it is suitable for the analysis of moisture diffusion in a heterogeneous composite material filled with permeable fibers.

To enforce continuity across a bi-material interface for modeling of moisture diffusion in a multi-material system, a moisture wetness variable, W, is introduced. W is defined as

$$W = \frac{C}{C_{sat}}, \quad 1 \geq W \geq 0. \tag{1}$$

where C and C_{sat} are, respectively, the moisture concentration and the maximum moisture concentration that can be absorbed by the material. The lower limit of W, i.e. $W = 0$, indicates that the material is completely dry, while the upper limit, i.e. $W = 1$, indicates that the material is fully saturated with moisture. The "wetness" thermal-moisture analogy scheme for the current finite element implementation is presented in Tab. 1.

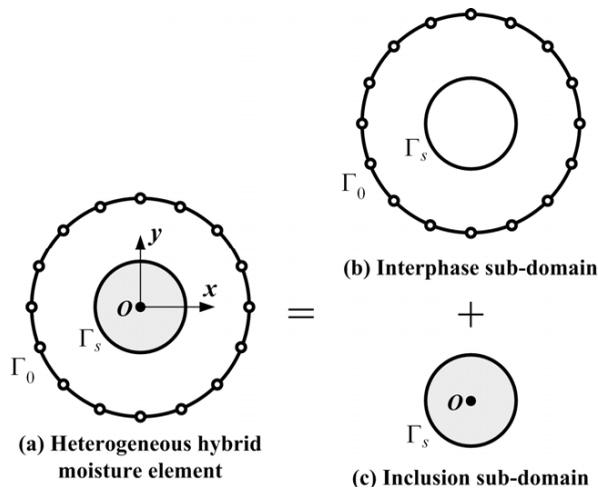Consider a 2-D plane region with a boundary s. The differential equation for the

Figure 1: Element decomposition: (a) heterogeneous hybrid moisture element; (b) inter-phase sub-domain; and (c) inclusion sub-domain

Table 1: FEA thermal-moisture analogy for moisture diffusion modeling

Properties	Thermal	Moisture
Field variable	Temperature, T	Wetness, W
Density	$\rho(\text{kg} / \text{m}^3)$	1
Conductivity	$K(\text{W} / \text{m} \cdot {}^\circ\text{C})$	$D * C_{\text{sat}}(\text{kg} / \text{s} \cdot \text{m})$
Specific capacity	$c(\text{J} / \text{kg} \cdot {}^\circ\text{C})$	$C_{\text{sat}}(\text{kg} / \text{m}^3)$

2-D moisture diffusion problem is given by

$$\frac{\partial W}{\partial x}\left(D_x \frac{\partial W}{\partial x}\right) + \frac{\partial W}{\partial y}\left(D_y \frac{\partial W}{\partial y}\right) = \frac{\partial W}{\partial t}. \tag{2}$$

and has boundary conditions of

$$W = W_0\,|_{s=s_D} \quad \text{and} \quad D_x n_x \frac{\partial W}{\partial x} + D_y n_y \frac{\partial W}{\partial y} = f_B\,|_{s=s_N}. \tag{3}$$

where D_x and D_y are the moisture diffusion coefficients for the x- and y-directions, respectively, n_x and n_y are directional cosines, and f_B is the boundary flux, which has a positive value when directed into the body of interest. Let s_D and s_N respectively denote the parts of s where the Dirichlet and Neumann boundary conditions are specified, where $s = s_D \cup s_N$ and $s_D \cap s_N = \emptyset$.

The unit element matrix equation can be obtained from the governing differential equation, Eq. (2), by applying Galerkin's weighted residual approach. The resulting element matrix equation has the form

$$[M_e]\{\dot{W}_e\} + [K_e]\{W_e\} = \{P_e\}, \tag{4}$$

in which the element moisture capacitance matrix is given by

$$[M_e] = \int [N]^T [N]\, dxdy, \tag{5}$$

the element moisture conductance matrix has the form

$$[K_e] = \int [B]^T [D][B]\, dxdy, \tag{6}$$

and finally

$$\{P_e\} = \int [N]^T f_B\, ds_N. \tag{7}$$

Note that in the equations above, $[B]$ and $[N]$ denote the shape function derivative matrix and the shape function matrix, respectively.

The diffusivity matrix is given by

$$[D] = \begin{bmatrix} D_x & 0 \\ 0 & D_y \end{bmatrix}.$$

(8)

For the time discretization of the system of ordinary differential equation, Eq. (4), we apply the well-know θ-method [Lewis, Morgan, Thomas and Seetharamu (1996)], which results in the equation

$$(M_e + \theta \cdot \Delta t \cdot K_e) \cdot W_e^{n+1} = [M_e - (1 - \theta) \cdot \Delta t \cdot K_e] \cdot W_e^n + \Delta t \cdot P_e.$$

(9)

Let $\phi = \theta - 1$ and substitute it into Eq. (9), get

$$(M_e + \theta \cdot \Delta t \cdot K_e) \cdot W_e^{n+1} = [M_e + \phi \cdot \Delta t \cdot K_e] \cdot W_e^n + \Delta t \cdot P_e,$$

(10)

where W_e^n denotes the known moisture wetness at the current time t_n, the time step increment Δt is defined as $\Delta t = t_{n+1} - t_n$ and $(M_e + \theta \cdot \Delta t \cdot K_e)$ denotes the combined moisture capacitance/conductance matrix. Clearly, this is a system of linear algebraic equations with respect to the unknown vector W_e^{n+1} as the approximation of the moisture wetness at the new time-level t_{n+1}. Here the parameter θ is related to the applied numerical method and is an arbitrary parameter on the interval [0, 1]. It is worth emphasizing that in $\theta = 0.5$, the method yields the Crank-Nicolson implicit method which produces a higher accuracy for time discretization [Crank and Nicolson (1947)]. Therefore, the parameter θ in the current numerical analysis is set as 0.5.

Another practical consideration was a proper time increment. If the time increment is not selected properly, the results can exhibit spurious numerical oscillation (if the time increment is too short). The guideline in Ref. [Hibbitt, Karlsson and Sorensen (2004)] suggests that the time step increment (Δt) should be slightly greater than $\Delta l^2 / (6 \cdot \theta \cdot D)$, where D is the diffusivity and Δl is a typical element dimension.

2.2 *2-D hybrid moisture element formulation*

In the formulation, the material properties are assumed to be linearly elastic and isotropic, but are heterogeneous from each sub-domain. As shown in Fig. 2, the radius of the inclusion sub-domain, r_{inc}, and the radius of the element domain, r, have the following relationship: $r_{inc} = r \times c^s$ where c is a specific compatible proportionality constant and s is a specific number of chosen element-layers in the inter-phase sub-domain. Then, the thickness of the inter-phase sub-domain is

$r - r_{inc}$. The separate formulations for the two sub-domains are derived (index notation is used) as follows:

(I) Formulation in the inter-phase sub-domain:

The similar partition concept [Guo (1979)] is applied to the inter-phase sub-domain, as shown in Fig. 2(a). The meshing steps are described as follows: First, the outer boundary (element domain boundary), Γ_0, is properly discretized with the total number of $2m$ master nodes (represented by symbol "o"), ordered in a counter-clockwise direction. Second, when the global origin O located in the inclusion region is chosen as a similar partition center, and when a certain number of chosen element-layers s and a certain compatible proportionality constant $c \in (0, 1)$ are taken, similar polygons $\Gamma_1, \Gamma_2, \cdots, \Gamma_s$ of Γ_0 are constructed with center O according to the proportionality constants $c^1, c^2, \cdots, c^s$, respectively. The region bounded between Γ_{i-1} and Γ_i is called the *i-th* element-layer ($i = 1, 2, \cdots, s$). Third, straight lines are drawn from the origin to the master nodes, and each individual Γ_i is regularly discretized, similar to Γ_0. The nodal number and coordinates of the nodes on each individual Γ_i can be determined from the master node coordinates under geometrically similar conditions. Fourth, each element-layer is auto-meshed into several four-node quadrilateral elements that are similar to one another from the element-layers in a radial direction.

Both the element moisture capacitance matrix $[M_e]$ and the element moisture conductance matrix $[K_e]$ for each quadrilateral element in the element layer of the inter-phase sub-domain (i.e. the region between boundaries Γ_0 and Γ_1) can be calculated and assembled into global matrices, i.e. $[M]$ and $[K]$, using the conventional finite element formulation. The assembled matrices of the outermost element-layer (1st element-layer) are therefore expressed as

$$[M] = \begin{bmatrix} M_a & -B^T \\ -B & M_b \end{bmatrix}_{2m \times 2m} \tag{11}$$

and

$$[K] = \begin{bmatrix} K_a & -A^T \\ -A & K_b \end{bmatrix}_{2m \times 2m}, \tag{12}$$

where M_a, M_b, and B are sub-matrices of the assembled matrix $[M]$ with identical dimensions $m \times m$, K_a, K_b, and A are sub-matrices of the assembled matrix $[K]$ with identical dimensions $m \times m$, and B^T and A^T are the transposes of B and A, respectively. Since the element layer matrices $[M]$ and $[K]$ are globally symmetrical and banded, matrices M_a, M_b, K_a, and K_b are also symmetrical and banded.

The nodal moisture wetness vector W_i^n of the nodes on Γ_i at the time t_n is defined
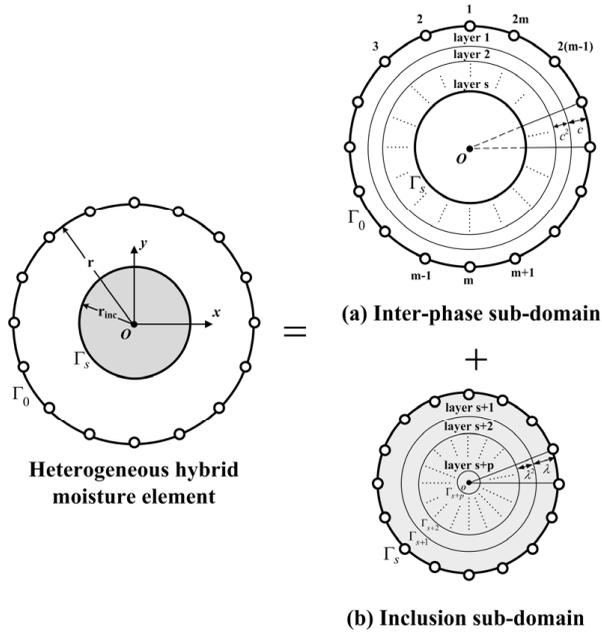
(a) Inter-phase sub-domain

+

(b) Inclusion sub-domain

Figure 2: Heterogeneous hybrid moisture element mesh: (a) inter-phase sub-domain; and (b) inclusion sub-domain

as

$$W_i^n \equiv \begin{bmatrix} W_1^{i,n} & W_2^{i,n} & \cdots & W_{2m}^{i,n} \end{bmatrix}^T . \tag{13}$$

The nodal loading vector P_i of the nodes on Γ_i is defined as

$$P_i \equiv \begin{bmatrix} P_1^i & P_2^i & \cdots & P_{2m}^i \end{bmatrix}^T . \tag{14}$$

According to the similarity principle, it is obvious that the element moisture capacitance matrices of all of the element-layers are in dimensional dependence on the ratio c^2 and the element moisture conductance matrices of all of the element-layers are identical. Hence, in accordance with Eq. (10), we can express the element matrices of the *s* element-layers (from the *1st* element-layer to the *s-th* element-layer) as *s* sets of algebraic equations, namely,

for layer 1

$$\begin{bmatrix} M_a + \theta \cdot \Delta t \cdot K_a & -B^T - \theta \cdot \Delta t \cdot A^T \\ -B - \theta \cdot \Delta t \cdot A & M_b + \theta \cdot \Delta t \cdot K_b \end{bmatrix} \cdot \begin{bmatrix} W_0^{n+1} \\ W_1^{n+1} \end{bmatrix}$$
$$= \begin{bmatrix} M_a + \phi \cdot \Delta t \cdot K_a & -B^T - \phi \cdot \Delta t \cdot A^T \\ -B - \phi \cdot \Delta t \cdot A & M_b + \phi \cdot \Delta t \cdot K_b \end{bmatrix} \cdot \begin{bmatrix} W_0^n \\ W_1^n \end{bmatrix} + \Delta t \cdot \begin{bmatrix} P_0 \\ P_1 \end{bmatrix} \tag{15}$$

for layer 2

$$
\begin{bmatrix} c^2 M_a + \theta \cdot \Delta t \cdot K_a & -c^2 B^T - \theta \cdot \Delta t \cdot A^T \\ -c^2 B - \theta \cdot \Delta t \cdot A & c^2 M_b + \theta \cdot \Delta t \cdot K_b \end{bmatrix} \cdot \begin{bmatrix} W_1^{n+1} \\ W_2^{n+1} \end{bmatrix}
$$
$$
= \begin{bmatrix} c^2 M_a + \phi \cdot \Delta t \cdot K_a & -c^2 B^T - \phi \cdot \Delta t \cdot A^T \\ -c^2 B - \phi \cdot \Delta t \cdot A & c^2 M_b + \phi \cdot \Delta t \cdot K_b \end{bmatrix} \cdot \begin{bmatrix} W_1^n \\ W_2^n \end{bmatrix} + \Delta t \cdot \begin{bmatrix} -P_1 \\ P_2 \end{bmatrix} \tag{16}
$$

for layer 3

$$
\begin{bmatrix} c^4 M_a + \theta \cdot \Delta t \cdot K_a & -c^4 B^T - \theta \cdot \Delta t \cdot A^T \\ -c^4 B - \theta \cdot \Delta t \cdot A & c^4 M_b + \theta \cdot \Delta t \cdot K_b \end{bmatrix} \cdot \begin{bmatrix} W_2^{n+1} \\ W_3^{n+1} \end{bmatrix}
$$
$$
= \begin{bmatrix} c^4 M_a + \phi \cdot \Delta t \cdot K_a & -c^4 B^T - \phi \cdot \Delta t \cdot A^T \\ -c^4 B - \phi \cdot \Delta t \cdot A & c^4 M_b + \phi \cdot \Delta t \cdot K_b \end{bmatrix} \cdot \begin{bmatrix} W_2^n \\ W_3^n \end{bmatrix} + \Delta t \cdot \begin{bmatrix} -P_2 \\ P_3 \end{bmatrix} \tag{17}
$$

for layer s

$$
\begin{bmatrix} c^{2(s-1)} M_a + \theta \cdot \Delta t \cdot K_a & -c^{2(s-1)} B^T - \theta \cdot \Delta t \cdot A^T \\ -c^{2(s-1)} B - \theta \cdot \Delta t \cdot A & c^{2(s-1)} M_b + \theta \cdot \Delta t \cdot K_b \end{bmatrix} \cdot \begin{bmatrix} W_{s-1}^{n+1} \\ W_s^{n+1} \end{bmatrix}
$$
$$
= \begin{bmatrix} c^{2(s-1)} M_a + \phi \cdot \Delta t \cdot K_a & -c^{2(s-1)} B^T - \phi \cdot \Delta t \cdot A^T \\ -c^{2(s-1)} B - \phi \cdot \Delta t \cdot A & c^{2(s-1)} M_b + \phi \cdot \Delta t \cdot K_b \end{bmatrix} \cdot \begin{bmatrix} W_{s-1}^n \\ W_s^n \end{bmatrix} + \Delta t \cdot \begin{bmatrix} -P_{s-1} \\ P_s \end{bmatrix} \tag{18}
$$

Extracting each algebraic equation, combining the second equation for the *i-th* element-layer, and the first equation for the *(i+1)-th* element-layer, and letting $X = M_b + c^2 M_a$ and $Y = K_b + K_a$, we have

$$
(M_a + \theta \cdot \Delta t \cdot K_a) \cdot W_0^{n+1} + \left(-B^T - \theta \cdot \Delta t \cdot A^T\right) \cdot W_1^{n+1}
$$
$$
= (M_a + \phi \cdot \Delta t \cdot K_a) \cdot W_0^n + \left(-B^T - \phi \cdot \Delta t \cdot A^T\right) \cdot W_1^n + \Delta t \cdot P_0 \tag{19}
$$

$$
(-B - \theta \cdot \Delta t \cdot A) \cdot W_0^{n+1} + (X + \theta \cdot \Delta t \cdot Y) \cdot W_1^{n+1} + \left(-c^2 B^T - \theta \cdot \Delta t \cdot A^T\right) \cdot W_2^{n+1}
$$
$$
= (-B - \phi \cdot \Delta t \cdot A) \cdot W_0^n + (X + \phi \cdot \Delta t \cdot Y) \cdot W_1^n + \left(-c^2 B^T - \phi \cdot \Delta t \cdot A^T\right) \cdot W_2^n \tag{20}
$$

$$\vdots$$

$$
\left(-c^{2(i-1)} B - \theta \cdot \Delta t \cdot A\right) \cdot W_{i-1}^{n+1} + \left(c^{2(i-1)} X + \theta \cdot \Delta t \cdot Y\right) \cdot W_i^{n+1}
$$
$$
+ \left(-c^{2i} B^T - \theta \cdot \Delta t \cdot A^T\right) \cdot W_{i+1}^{n+1} = \left(-c^{2(i-1)} B - \phi \cdot \Delta t \cdot A\right) \cdot W_{i-1}^n
$$
$$
+ \left(c^{2(i-1)} X + \phi \cdot \Delta t \cdot Y\right) \cdot W_i^n + \left(-c^{2i} B^T - \phi \cdot \Delta t \cdot A^T\right) \cdot W_{i+1}^n \tag{21}
$$

$$\vdots$$

$$
\left(-c^{2(s-2)} B - \theta \cdot \Delta t \cdot A\right) \cdot W_{s-2}^{n+1} + \left(c^{2(s-2)} X + \phi \cdot \Delta t \cdot Y\right) \cdot W_{s-1}^{n+1}
$$
$$
+ \left(-c^{2(s-1)} B^T - \theta \cdot \Delta t \cdot A^T\right) \cdot W_s^{n+1} = \left(-c^{2(s-2)} B - \phi \cdot \Delta t \cdot A\right) \cdot W_{s-2}^n
$$
$$
+ \left(c^{2(s-2)} X + \phi \cdot \Delta t \cdot Y\right) \cdot W_{s-1}^n + \left(-c^{2(s-1)} B^T - \phi \cdot \Delta t \cdot A^T\right) \cdot W_s^n \tag{22}
$$

$$\left(-c^{2(s-1)}B - \theta \cdot \Delta t \cdot A\right) \cdot W_{s-1}^{n+1} + \left(c^{2(s-1)}M_b + \theta \cdot \Delta t \cdot K_b\right) \cdot W_s^{n+1}$$
$$= \left(-c^{2(s-1)}B - \phi \cdot \Delta t \cdot A\right) \cdot W_{s-1}^n + \left(c^{2(s-1)}M_b + \phi \cdot \Delta t \cdot K_b\right) \cdot W_s^n + \Delta t \cdot P_s \tag{23}$$

(II) Formulation in the inclusion sub-domain:

The partition processes for the inclusion sub-domain, as shown in Fig. 2(b), are similar to the processes for the inter-phase sub-domain. The inner boundary Γ_s of the inter-phase region is exactly the outer boundary of the inclusion region. Also, when the global origin O is chosen as the similar partition center and when another proportionality constant λ and element-layers p are taken, similar polygons Γ_{s+1}, Γ_{s+2}, $\cdots$, Γ_{s+p} of Γ_s are generated with center O, according to the relative proportionality constants λ^1, λ^2, $\cdots$, λ^p. The region bounded between Γ_{j-1} and Γ_j is called the *j-th* element-layer (j= s+1, s+2, $\cdots$, s + p). The assembled matrices of the p element-layers (from the *s+1-th* element-layer to the *s+p-th* element-layer) can be expressed as p sets of algebraic equations, namely,

for layer $s+1$

$$\begin{bmatrix} M_{\Delta a} + \theta \cdot \Delta t \cdot K_{\Delta a} & -B_\Delta^T - \theta \cdot \Delta t \cdot A_\Delta^T \\ -B_\Delta - \theta \cdot \Delta t \cdot A_\Delta & M_{\Delta b} + \theta \cdot \Delta t \cdot K_{\Delta b} \end{bmatrix} \cdot \begin{bmatrix} W_s^{n+1} \\ W_{s+1}^{n+1} \end{bmatrix}$$
$$= \begin{bmatrix} M_{\Delta a} + \phi \cdot \Delta t \cdot K_{\Delta a} & -B_\Delta^T - \phi \cdot \Delta t \cdot A_\Delta^T \\ -B_\Delta - \phi \cdot \Delta t \cdot A_\Delta & M_{\Delta b} + \phi \cdot \Delta t \cdot K_{\Delta b} \end{bmatrix} \cdot \begin{bmatrix} W_s^n \\ W_{s+1}^n \end{bmatrix} + \Delta t \cdot \begin{bmatrix} -P_s \\ P_{s+1} \end{bmatrix} \tag{24}$$

for layer $s+2$

$$\begin{bmatrix} \lambda^2 M_{\Delta a} + \theta \cdot \Delta t \cdot K_{\Delta a} & -\lambda^2 B_\Delta^T - \theta \cdot \Delta t \cdot A_\Delta^T \\ -\lambda^2 B_\Delta - \theta \cdot \Delta t \cdot A_\Delta & \lambda^2 M_{\Delta b} + \theta \cdot \Delta t \cdot K_{\Delta b} \end{bmatrix} \cdot \begin{bmatrix} W_{s+1}^{n+1} \\ W_{s+2}^{n+1} \end{bmatrix}$$
$$= \begin{bmatrix} \lambda^2 M_{\Delta a} + \phi \cdot \Delta t \cdot K_{\Delta a} & -\lambda^2 B_\Delta^T - \phi \cdot \Delta t \cdot A_\Delta^T \\ -\lambda^2 B_\Delta - \phi \cdot \Delta t \cdot A_\Delta & \lambda^2 M_{\Delta b} + \phi \cdot \Delta t \cdot K_{\Delta b} \end{bmatrix} \cdot \begin{bmatrix} W_{s+1}^n \\ W_{s+2}^n \end{bmatrix} + \Delta t \cdot \begin{bmatrix} -P_{s+1} \\ P_{s+2} \end{bmatrix} \tag{25}$$

for layer $s+3$

$$\begin{bmatrix} \lambda^4 M_{\Delta a} + \theta \cdot \Delta t \cdot K_{\Delta a} & -\lambda^4 B_\Delta^T - \theta \cdot \Delta t \cdot A_\Delta^T \\ -\lambda^4 B_\Delta - \theta \cdot \Delta t \cdot A_\Delta & \lambda^4 M_{\Delta b} + \theta \cdot \Delta t \cdot K_{\Delta b} \end{bmatrix} \cdot \begin{bmatrix} W_{s+2}^{n+1} \\ W_{s+3}^{n+1} \end{bmatrix}$$
$$= \begin{bmatrix} \lambda^4 M_{\Delta a} + \phi \cdot \Delta t \cdot K_{\Delta a} & -\lambda^4 B_\Delta^T - \phi \cdot \Delta t \cdot A_\Delta^T \\ -\lambda^4 B_\Delta - \phi \cdot \Delta t \cdot A_\Delta & \lambda^4 M_{\Delta b} + \phi \cdot \Delta t \cdot K_{\Delta b} \end{bmatrix} \cdot \begin{bmatrix} W_{s+2}^n \\ W_{s+3}^n \end{bmatrix} + \Delta t \cdot \begin{bmatrix} -P_{s+2} \\ P_{s+3} \end{bmatrix} \tag{26}$$

$\vdots$ for layer s + p

$$\begin{bmatrix} \lambda^{2(p-1)} M_{\Delta a} + \theta \cdot \Delta t \cdot K_{\Delta a} & -\lambda^{2(p-1)} B_\Delta^T - \theta \cdot \Delta t \cdot A_\Delta^T \\ -\lambda^{2(p-1)} B_\Delta - \theta \cdot \Delta t \cdot A_\Delta & \lambda^{2(p-1)} M_{\Delta b} + \theta \cdot \Delta t \cdot K_{\Delta b} \end{bmatrix} \cdot \begin{bmatrix} W_{s+p-1}^{n+1} \\ W_{s+p}^{n+1} \end{bmatrix}$$
$$= \begin{bmatrix} \lambda^{2(p-1)} M_{\Delta a} + \phi \cdot \Delta t \cdot K_{\Delta a} & -\lambda^{2(p-1)} B_\Delta^T - \phi \cdot \Delta t \cdot A_\Delta^T \\ -\lambda^{2(p-1)} B_\Delta - \phi \cdot \Delta t \cdot A_\Delta & \lambda^{2(p-1)} M_{\Delta b} + \phi \cdot \Delta t \cdot K_{\Delta b} \end{bmatrix} \cdot \begin{bmatrix} W_{s+p-1}^n \\ W_{s+p}^n \end{bmatrix}$$
$$+ \Delta t \cdot \begin{bmatrix} -P_{s+p-1} \\ P_{s+p} \end{bmatrix} \tag{27}$$

Extracting each algebraic equation, combining the second equation for the *j-th* element-layer and the first equation for the *(j+1)-th* element-layer, and letting $R = M_{\Delta b} + \lambda^2 M_{\Delta a}$ and $Q = K_{\Delta b} + K_{\Delta a}$, we have

$$
(M_{\Delta a} + \theta \cdot \Delta t \cdot K_{\Delta a}) \cdot W_s^{n+1} + \left(-B_\Delta^T - \theta \cdot \Delta t \cdot A_\Delta^T\right) \cdot W_{s+1}^{n+1}
= (M_{\Delta a} + \phi \cdot \Delta t \cdot K_{\Delta a}) \cdot W_s^n + \left(-B_\Delta^T - \phi \cdot \Delta t \cdot A_\Delta^T\right) \cdot W_{s+1}^n - \Delta t \cdot P_s
\tag{28}
$$

$$
(-B_\Delta - \theta \cdot \Delta t \cdot A_\Delta) \cdot W_s^{n+1} + (R + \theta \cdot \Delta t \cdot Q) \cdot W_{s+1}^{n+1} + \left(-\lambda^2 B_\Delta^T - \theta \cdot \Delta t \cdot A_\Delta^T\right) \cdot W_{s+2}^{n+1}
= (-B_\Delta - \phi \cdot \Delta t \cdot A_\Delta) \cdot W_s^n + (R + \phi \cdot \Delta t \cdot Q) \cdot W_{s+1}^n + \left(-\lambda^2 B_\Delta^T - \phi \cdot \Delta t \cdot A_\Delta^T\right) \cdot W_{s+2}^n
\tag{29}
$$

$$\vdots$$

$$
\left(-\lambda^{2(j-(s+1))} B_\Delta - \theta \cdot \Delta t \cdot A_\Delta\right) \cdot W_{j-1}^{n+1} + \left(\lambda^{2(j-(s+1))} R + \theta \cdot \Delta t \cdot Q\right) \cdot W_j^{n+1}
+ \left(-\lambda^{2(j-s)} B_\Delta^T - \theta \cdot \Delta t \cdot A_\Delta^T\right) \cdot W_{j+1}^{n+1} = \left(-\lambda^{2(j-(s+1))} B_\Delta - \phi \cdot \Delta t \cdot A_\Delta\right) \cdot W_{j-1}^n
+ \left(\lambda^{2(j-(s+1))} R + \phi \cdot \Delta t \cdot Q\right) \cdot W_j^n + \left(-\lambda^{2(j-s)} B_\Delta^T - \phi \cdot \Delta t \cdot A_\Delta^T\right) \cdot W_{j+1}^n
\tag{30}
$$

$$\vdots$$

$$
\left(-\lambda^{2(p-2)} B_\Delta - \theta \cdot \Delta t \cdot A_\Delta\right) \cdot W_{s+p-2}^{n+1} + \left(\lambda^{2(p-2)} R + \theta \cdot \Delta t \cdot Q\right) \cdot W_{s+p-1}^{n+1}
+ \left(-\lambda^{2(p-1)} B_\Delta^T - \theta \cdot \Delta t \cdot A_\Delta^T\right) \cdot W_{s+p}^{n+1} = \left(-\lambda^{2(p-2)} B_\Delta - \phi \cdot \Delta t \cdot A_\Delta\right) \cdot W_{s+p-2}^n
+ \left(\lambda^{2(p-2)} R + \phi \cdot \Delta t \cdot Q\right) \cdot W_{s+p-1}^n + \left(-\lambda^{2(p-1)} B_\Delta^T - \phi \cdot \Delta t \cdot A_\Delta^T\right) \cdot W_{s+p}^n
\tag{31}
$$

$$
\left(-\lambda^{2(p-1)} B_\Delta - \theta \cdot \Delta t \cdot A_\Delta\right) \cdot W_{s+p-1}^{n+1} + \left(\lambda^{2(p-1)} M_{\Delta b} + \theta \cdot \Delta t \cdot K_{\Delta b}\right) \cdot W_{s+p}^{n+1}
= \left(-\lambda^{2(p-1)} B_\Delta - \phi \cdot \Delta t \cdot A_\Delta\right) \cdot W_{s+p-1}^n + \left(\lambda^{2(p-1)} M_{\Delta b} + \phi \cdot \Delta t \cdot K_{\Delta b}\right) \cdot W_{s+p}^n
+ \Delta t \cdot P_{s+p}
\tag{32}
$$

Let $N_{s+p} = \lambda^{2(p-1)} M_{\Delta b} + \phi \cdot \Delta t \cdot K_{\Delta b}$, $V_{s+p} = \lambda^{2(p-1)} M_{\Delta b} + \theta \cdot \Delta t \cdot K_{\Delta b}$ and $FF_{s+p} = \Delta t \cdot P_{s+p}$. Substituting them into Eq. (32), we have

$$
W_{s+p}^{n+1} = -V_{s+p}^{-1} \cdot \left(-\lambda^{2(p-1)} B_\Delta - \theta \cdot \Delta t \cdot A_\Delta\right) \cdot W_{s+p-1}^{n+1}
+ V_{s+p}^{-1} \cdot \left[\left(-\lambda^{2(p-1)} B_\Delta - \phi \cdot \Delta t \cdot A_\Delta\right) \cdot W_{s+p-1}^n + N_{s+p} \cdot W_{s+p}^n + FF_{s+p}\right]
\tag{33}
$$

By substituting Eq. (33) into Eq. (31), we get

$$
\left(-\lambda^{2(p-2)} B_\Delta - \theta \cdot \Delta t \cdot A_\Delta\right) \cdot W_{s+p-2}^{n+1}
+ \left[\begin{array}{l}
\left(\lambda^{2(p-2)} R + \theta \cdot \Delta t \cdot Q\right) \\
- \left(-\lambda^{2(p-1)} B_\Delta^T - \theta \cdot \Delta t \cdot A_\Delta^T\right) \cdot V_{s+p}^{-1} \cdot \left(-\lambda^{2(p-1)} B_\Delta - \theta \cdot \Delta t \cdot A_\Delta\right)
\end{array}\right] \cdot W_{s+p-1}^{n+1}
= \left(-\lambda^{2(p-2)} B_\Delta - \phi \cdot \Delta t \cdot A_\Delta\right) \cdot W_{s+p-2}^n + \left(\lambda^{2(p-2)} R + \phi \cdot \Delta t \cdot Q\right) \cdot W_{s+p-1}^n
+ \left(-\lambda^{2(p-1)} B_\Delta^T - \phi \cdot \Delta t \cdot A_\Delta^T\right) \cdot W_{s+p}^n
- \left(-\lambda^{2(p-1)} B_\Delta^T - \theta \cdot \Delta t \cdot A_\Delta^T\right) \cdot V_{s+p}^{-1} \cdot \left[\begin{array}{l}
\left(-\lambda^{2(p-1)} B_\Delta - \phi \cdot \Delta t \cdot A_\Delta\right) \cdot W_{s+p-1}^n \\
+ N_{s+p} \cdot W_{s+p}^n + FF_{s+p}
\end{array}\right]
$$

$$\tag{34}$$

When Eq. (34) is compared with Eq. (32), three iteration formulas can be inferred:

$$N_i = \lambda^{2(i-(s+1))}R + \phi \cdot \Delta t \cdot Q \tag{35}$$

$$
\begin{aligned}
V_i &= \lambda^{2(i-(s+1))}R + \theta \cdot \Delta t \cdot Q \\
&\quad - \left(-\lambda^{2(i-s)}B_\Delta^T - \theta \cdot \Delta t \cdot A_\Delta^T\right) \cdot (V_{i+1})^{-1} \cdot \left(-\lambda^{2(i-s)}B_\Delta - \theta \cdot \Delta t \cdot A_\Delta\right)
\end{aligned}
\tag{36}
$$

$$
\begin{aligned}
FF_i^n &= \left(-\lambda^{2(i-s)}B_\Delta^T - \phi \cdot \Delta t \cdot A_\Delta^T\right) \cdot W_{i+1}^n \\
&\quad - \left(-\lambda^{2(i-s)}B_\Delta^T - \theta \cdot \Delta t \cdot A_\Delta^T\right) \cdot (V_{i+1})^{-1} \cdot \left[\begin{array}{l} \left(-\lambda^{2(i-s)}B_\Delta - \phi \cdot \Delta t \cdot A_\Delta\right) \cdot W_i^n \\ + (N_{i+1}) \cdot W_{i+1}^n + FF_{i+1} \end{array} \right]
\end{aligned}
\tag{37}
$$

where $i = s+1,\ s+2,\ s+3, \cdots, s+p\text{-}1$.

By substituting the above three iteration formulas into Eq. (34), we get

$$
\begin{aligned}
&\left(-\lambda^{2(p-2)}B_\Delta - \theta \cdot \Delta t \cdot A_\Delta\right) \cdot W_{s+p-2}^{n+1} + V_{s+p-1} \cdot W_{s+p-1}^{n+1} \\
&= \left(-\lambda^{2(p-2)}B_\Delta - \phi \cdot \Delta t \cdot A_\Delta\right) \cdot W_{s+p-2}^n + N_{s+p-1} \cdot W_{s+p-1}^n + FF_{s+p-1}
\end{aligned}
\tag{38}
$$

Rearranging Eq. (38) and another iteration formula can be inferred as

$$
\begin{aligned}
W_j^{n+1} &= -V_j^{-1} \cdot \left(-\lambda^{2(j-(s+1))}B_\Delta - \theta \cdot \Delta t \cdot A_\Delta\right) \cdot W_{j-1}^{n+1} \\
&\quad + V_j^{-1} \cdot \left[\left(-\lambda^{2(j-(s+1))}B_\Delta - \phi \cdot \Delta t \cdot A_\Delta\right) \cdot W_{j-1}^n + N_j \cdot W_j^n + FF_j\right]
\end{aligned}
\tag{39}
$$

where $j = s+1,\ s+2,\ s+3, \cdots, s+p$.

From Eq. (39), we have

$$
\begin{aligned}
W_{s+1}^{n+1} &= -V_{s+1}^{-1} \cdot \left(-B_\Delta - \theta \cdot \Delta t \cdot A_\Delta\right) \cdot W_s^{n+1} \\
&\quad + V_{s+1}^{-1} \cdot \left[\left(-B_\Delta - \phi \cdot \Delta t \cdot A_\Delta\right) \cdot W_s^n + N_{s+1} \cdot W_{s+1}^n + FF_{s+1}\right]
\end{aligned}
\tag{40}
$$

By substituting Eq. (40) into Eq. (28), we get

$$
\begin{aligned}
&(M_{\Delta a} + \theta \cdot \Delta t \cdot K_{\Delta a}) \cdot W_s^{n+1} \\
&+ \left(-B_\Delta^T - \theta \cdot \Delta t \cdot A_\Delta^T\right) \cdot \left\{ \begin{array}{l} -V_{s+1}^{-1} \cdot \left(-B_\Delta - \theta \cdot \Delta t \cdot A_\Delta\right) \cdot W_s^{n+1} \\ +V_{s+1}^{-1} \cdot \left[\left(-B_\Delta - \phi \cdot \Delta t \cdot A_\Delta\right) \cdot W_s^n + N_{s+1} \cdot W_{s+1}^n + FF_{s+1}\right] \end{array} \right\} \\
&= (M_{\Delta a} + \phi \cdot \Delta t \cdot K_{\Delta a}) \cdot W_s^n + \left(-B_\Delta^T - \phi \cdot \Delta t \cdot A_\Delta^T\right) \cdot W_{s+1}^n - \Delta t \cdot P_s
\end{aligned}
\tag{41}
$$

Rearranging Eq. (41), we have

$$
\begin{aligned}
&\left[(M_{\Delta a} + \theta \cdot \Delta t \cdot K_{\Delta a}) - \left(-B_\Delta^T - \theta \cdot \Delta t \cdot A_\Delta^T\right) \cdot V_{s+1}^{-1} \cdot \left(-B_\Delta - \theta \cdot \Delta t \cdot A_\Delta\right)\right] \cdot W_s^{n+1} \\
&= (M_{\Delta a} + \phi \cdot \Delta t \cdot K_{\Delta a}) \cdot W_s^n + \left(-B_\Delta^T - \phi \cdot \Delta t \cdot A_\Delta^T\right) \cdot W_{s+1}^n - \Delta t \cdot P_s \\
&\quad - \left(-B_\Delta^T - \theta \cdot \Delta t \cdot A_\Delta^T\right) \cdot V_{s+1}^{-1} \cdot \left[\left(-B_\Delta - \phi \cdot \Delta t \cdot A_\Delta\right) \cdot W_s^n + N_{s+1} \cdot W_{s+1}^n + FF_{s+1}\right]
\end{aligned}
$$

$$(42)$$

Equation (42) can be expressed in the concise form

$$
H_{(\text{inclusion})} \cdot W_s^{n+1} = F_{(\text{inclusion})}
\tag{43}
$$

where $H_{(\text{inclusion})}$ and $F_{(\text{inclusion})}$ denote the equivalent hybrid moisture capacitance/-conductance matrix and associated loading vector for the inclusion sub-domain, respectively. Along the inclusion/inter-phase interface Γ_s, however, the moisture wetness compatibility and force equilibrium must be satisfied. Therefore, equations (23) and (43) are combined and we have

$$
\begin{aligned}
&\left(-c^{2(s-1)}B - \theta \cdot \Delta t \cdot A\right) \cdot W_{s-1}^{n+1} + \left[\left(c^{2(s-1)}M_b + \theta \cdot \Delta t \cdot K_b\right) + H_{(\text{inclusion})}\right] \cdot W_s^{n+1} \\
&= \left(-c^{2(s-1)}B - \phi \cdot \Delta t \cdot A\right) \cdot W_{s-1}^n + \left[c^{2(s-1)}M_b + M_{\Delta a} + \phi \cdot \Delta t \cdot (K_b + K_{\Delta a})\right] \cdot W_s^n \\
&\quad + \left(-B_\Delta^T - \phi \cdot \Delta t \cdot A_\Delta^T\right) \cdot W_{s+1}^n \\
&\quad - \left(-B_\Delta^T - \theta \cdot \Delta t \cdot A_\Delta^T\right) \cdot V_{s+1}^{-1} \cdot \left[\begin{array}{c} \left(-B_\Delta - \phi \cdot \Delta t \cdot A_\Delta\right) \cdot W_s^n \\ + N_{s+1} \cdot W_{s+1}^n + FF_{s+1} \end{array}\right]
\end{aligned}
$$

$$(44)$$

Again, let

$$
N_s = c^{2(s-1)}M_b + M_{\Delta a} + \phi \cdot \Delta t \cdot (K_b + K_{\Delta a}),
$$

$$
V_s = \left(c^{2(s-1)}M_b + \theta \cdot \Delta t \cdot K_b\right) + H_{(\text{inclusion})}
$$

and

$$
\begin{aligned}
FF_s &= \left(-B_\Delta^T - \phi \cdot \Delta t \cdot A_\Delta^T\right) \cdot W_{s+1}^n \\
&\quad - \left(-B_\Delta^T - \theta \cdot \Delta t \cdot A_\Delta^T\right) \cdot V_{s+1}^{-1} \cdot \left[\left(-B_\Delta - \phi \cdot \Delta t \cdot A_\Delta\right) \cdot W_s^n + N_{s+1} \cdot W_{s+1}^n + FF_{s+1}\right]
\end{aligned} \quad .
$$

Four parameters representing the inter-phase sub-domain can be inferred:

$$
N_i = c^{2(i-1)}X + \phi \cdot \Delta t \cdot Y
\tag{45}
$$

$$
V_i = c^{2(i-1)}X + \theta \cdot \Delta t \cdot Y - \left(-c^{2i}B^T - \theta \cdot \Delta t \cdot A^T\right) \cdot (V_{i+1})^{-1} \cdot \left(-c^{2i}B - \theta \cdot \Delta t \cdot A\right)
$$

$$(46)$$

$$FF_i = \left(-c^{2i}B^T - \phi \cdot \Delta t \cdot A^T\right) \cdot W_{i+1}^n$$
$$- \left(-c^{2i}B^T - \theta \cdot \Delta t \cdot A^T\right) \cdot (V_{i+1})^{-1} \cdot \left[\begin{array}{c} \left(-c^{2i}B - \phi \cdot \Delta t \cdot A\right) \cdot W_i^n \\ + (N_{i+1}) \cdot W_{i+1}^n + FF_{i+1} \end{array} \right] \tag{47}$$

$$W_j^{n+1} = -V_j^{-1} \cdot \left(-c^{2(i-1)}B - \theta \cdot \Delta t \cdot A\right) \cdot W_{j-1}^{n+1}$$
$$+ V_j^{-1} \cdot \left[\left(-c^{2(i-1)}B - \phi \cdot \Delta t \cdot A\right) \cdot W_{j-1}^n + N_j \cdot W_j^n + FF_j\right] \tag{48}$$

where $i = 1, 2, 3, \cdots, s$-1; and $j = 1, 2, 3, \cdots, s$.

Since N_s, V_s and FF_s are known, then N_{s-1}, N_{s-2}, $\cdots$, N_1; V_{s-1}, V_{s-2}, $\cdots$, V_1; FF_{s-1}, FF_{s-2}, $\cdots$, FF_1 can be iterated out using equations (45), (46) and (47), respectively. From Eq. (48), we have the unknown moisture wetness $W_1^{n+1} = -V_1^{-1} \cdot \left(-B - \theta \cdot \Delta t \cdot A\right) \cdot W_0^{n+1} + V_1^{-1} \cdot \left[\left(-B - \phi \cdot \Delta t \cdot A\right) \cdot W_0^n + N_1 \cdot W_1^n + FF_1\right]$ at the new time-level t_{n+1}. By substituting W_1^{n+1} into Eq. (19), we obtain the most important equation, that is,

$$\left[(M_a + \theta \cdot \Delta t \cdot K_a) - \left(-B^T - \theta \cdot \Delta t \cdot A^T\right) \cdot V_1^{-1} \cdot \left(-B - \theta \cdot \Delta t \cdot A\right)\right] \cdot W_0^{n+1}$$
$$= \left[(M_a + \phi \cdot \Delta t \cdot K_a) \cdot W_0^n + \left(-B^T - \phi \cdot \Delta t \cdot A^T\right) \cdot W_1^n + \Delta t \cdot P_0\right] \tag{49}$$
$$- \left(-B^T - \theta \cdot \Delta t \cdot A^T\right) \cdot V_1^{-1} \cdot \left[\left(-B - \phi \cdot \Delta t \cdot A\right) \cdot W_0^n + N_1 \cdot W_1^n + FF_1\right]$$

Equation (49) can be expressed in the concise form

$$H_Z \cdot W_0^{n+1} = F_Z \tag{50}$$

where H_Z and F_Z denote the equivalent hybrid moisture capacitance/conductance matrix and associated loading vector for the heterogeneous hybrid moisture element, respectively. The H_Z term preserves the symmetry characteristic of the global hybrid moisture capacitance/conductance matrix in FE representation. The F_Z term contains both effects of the outer surface traction and the known moisture wetness at the current time t_n. Once F_Z is determined, W_0^{n+1} can be obtained from Eq. (49). Then W_1^{n+1}, W_2^{n+1}, $\cdots$, W_s^{n+1}, $\cdots$, and W_{s+p}^{n+1} can be obtained sequentially from equations (48) and (39).

In the current analysis, it is assumed that the boundary flux is zero and that only the Dirichlet boundary condition is applied, i.e. concentrations only are prescribed at the boundaries. Therefore, the element matrix equation can be rewritten as:

$$\left[(M_a + \theta \cdot \Delta t \cdot K_a) - \left(-B^T - \theta \cdot \Delta t \cdot A^T\right) \cdot V_1^{-1} \cdot \left(-B - \theta \cdot \Delta t \cdot A\right)\right] \cdot W_0^{n+1}$$
$$= \left[(M_a + \phi \cdot \Delta t \cdot K_a) \cdot W_0^n + \left(-B^T - \phi \cdot \Delta t \cdot A^T\right) \cdot W_1^n\right] \tag{51}$$
$$- \left(-B^T - \theta \cdot \Delta t \cdot A^T\right) \cdot V_1^{-1} \cdot \left[\left(-B - \phi \cdot \Delta t \cdot A\right) \cdot W_0^n + N_1 \cdot W_1^n + FF_1\right]$$

where $P_i = 0$ ($i = 1, 2, \cdots, s, s+1, \cdots, s+p$).

2.3   Implementation of coupled HHME-FE scheme

The HHMEM is derived from the conventional FEM in space discretization as well as the θ-method in time discretization. Then it uses the similarity characteristic of element mass/stiffness and the matrix condensing procedures to solve transient moisture diffusion problems in heterogeneous materials and structures. A series of layer-wise elements with similar shapes are virtually generated within the problem domain. The numerous resultant degrees of freedom (DOFs) are condensed and transformed to those on the boundary master nodes only by means of derived recurrence formulas.

When the problem domain includes multiple sub-domains with repetitive geometry (for example, fiber inclusions), it is not favorable to employ finite elements to model an entire domain with a large number of elements. Therefore, we propose a coupled HHME-FE scheme that uses only HHMEs to subdivide the entire domain into several sub-domains without the use of finite elements. To illustrate the assembling scheme shown in Fig. 3, the global model is partitioned into two separate domains which are separated from the coupling interface Γ_0, namely Ω and D, modeled using the HHME and FE, respectively. The master nodes on the outer boundary of the HHMEs are taken from interface common nodes between the HHME and FE sub-domains. Because each HHME equivalent hybrid moisture capacitance/conductance matrix, H_Z, is pre-determined (see Section 2.2), the elements can be treated as regular finite elements, and their HHME H_Z matrices are assembled into the global combined capacitance/conductance matrix.

The related HHMEM numerical procedures and the coupled HHME-FE scheme were programmed and executed using self-written codes in MATLAB language [Kwon and Bang (2000)]. In the proposed approach, the total number of DOFs is remarkably reduced, and hence the modeling and computational effort are substantially decreased.
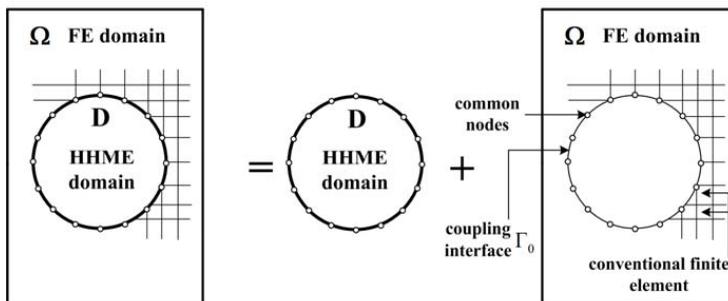

Figure 3: Schematic diagram of the coupled HHME-FE scheme

3   Validation of HHME-FE model

This section presents two examples in order to validate the performance of the proposed HHME-FE modeling approach.

Fig. 4 (right panel) shows the HHME-FE computational model with 3 inclusions and length and width dimensions (that is, the length to width ratio is 3:2). In this figure, D represents the HHME sub-domain and Ω represents the FE sub-domain. The HHME domain is separated into two regions containing the inclusion region (that is, the fibers) and the inter-phase region. The material properties of the inter-phase region are identical to those in the FE sub-domain (that is, the resin matrix). Therefore, the inter-phase is not explicitly modeled and it is assumed that a perfect bonding exists between the fibers and the resin matrix. As shown, the inclusions are circular, and have a radius 6.25 times smaller than the model length. A moisture condition of 35ºC/85% RH is applied at the left edge and hence the moisture permeates from the exposed surface on the left of the model and diffuses toward the right. Zero normal gradient conditions are used on the top, bottom and right edges. The moisture related material properties of the resin matrix and permeable fibers under the applied moisture conditions of 35ºC/85% RH are presented in Tab. 2 [Laurenzi, Albrizio and Marchetti (2008)].

Table 2: Material properties

Property	Fibers	Resin matrix
Moisture diffusivity (35ºC/85% RH)	3.631×10^{-14} m^2 / s	5.183×10^{-13} m^2 / s
Saturated moisture concentration (35ºC/85% RH)	2.375 kg / m^3	9.386 kg / m^3

The right panels of Fig. 4-6 show the coupled HHME-FE modeling results for the moisture profiles at three different time steps. The HHMEM parameters of the inclusion and inter-phase regions are, respectively: $\lambda = 0.5$ and $c = 0.833$; and $p = 5$ and $s = 1$. In the HHME-FE model, a total of 108 master nodes are used, with 36 nodes on each of the 3 HHME sub-domains, and 371 four-node quadrilateral elements in the FE sub-domain. The corresponding results obtained from the conventional FEM scheme are presented in the left panels for comparison purposes. In the conventional FE model, the number of elements totaled 1019 and the total number of nodes equaled 1010. Tab. 3 shows the comparisons of both methods by number of DOFs. Comparing the two sets of transient moisture distributions, it is apparent that the HHME-FE results are in favorable agreement
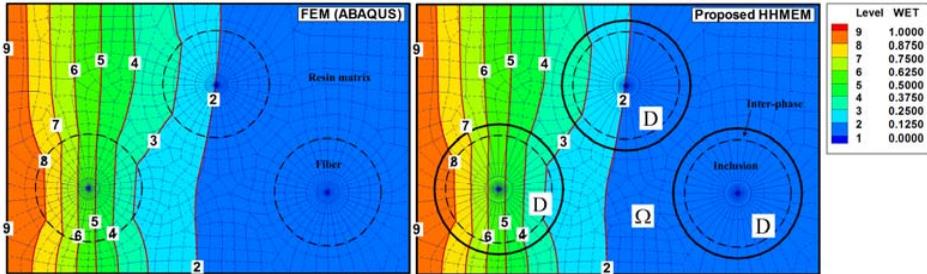
with the FEM results.

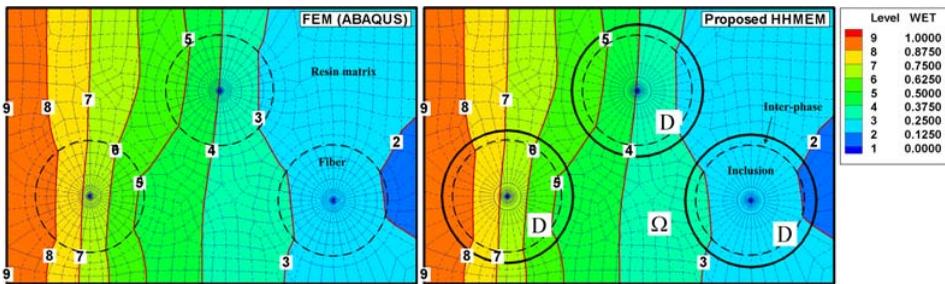Figure 4: Moisture distribution at the 80th time step for moisture conditions of 35ºC/85% RH

Figure 5: Moisture distribution at the 240th time step for moisture conditions of 35ºC/85% RH
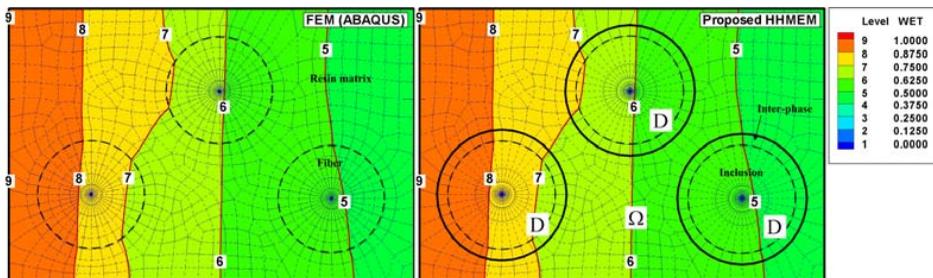

Figure 6: Moisture distribution at the 600th time step for moisture conditions of 35ºC/85% RH

Table 3: DOFs of the HHME-FE and FEM approaches

Numerical method	Total nodes	Total DOFs	Equivalent DOFs
HHME-FE	467	467	1115
FEM (ABAQUS)	1010	1010	1010

In the second validation example, Fig. 7 plots the variation for the level of wetness in the resin matrix after various time steps in an HHME-FE computational model with a length to thickness ratio of 5:1 and a 27% volume fraction of fibers. The time step increment is 180 s. The boundary conditions are the same as those of the first validation example. The HHMEM parameters of the inclusion and inter-phase regions are, respectively: $\lambda = 0.5$ and $c = 0.777$; and $p = 3$ and $s = 1$. In the HHME-FE model, a total of 1056 master nodes are used, with 12 nodes on each of the 88 HHME sub-domains, and 1136 four-node quadrilateral elements in the FE sub-domain. In the conventional FE model, the number of elements totaled 6416 and the total number of nodes was 5994. Tab. 4 shows the comparisons between both methods by number of DOFs. It can be seen that the results obtained from the HHME-FE method are in very favorable agreement with those obtained from the FEM approach and that the HHME-FE method contains many fewer DOFs than does the full FEM.

As described previously, the proposed HHMEM provides a straightforward and efficient means of modeling transient moisture diffusion in resin matrix filled with multiple fibers. This is due to the fact that only one HHME equivalent hybrid moisture capacitance/conductance matrix needs to be calculated for all HHMEs with the same properties. Furthermore, all DOFs related to the HHME domain are condensed and transformed to form a combined element with master node DOFs only. Therefore, the coupled HHME-FE method significantly reduces the execution time in the mesh modeling stage, the total number of DOFs, and the PC memory storage requirements.

Table 4: DOFs of the HME-FE and FEM approaches

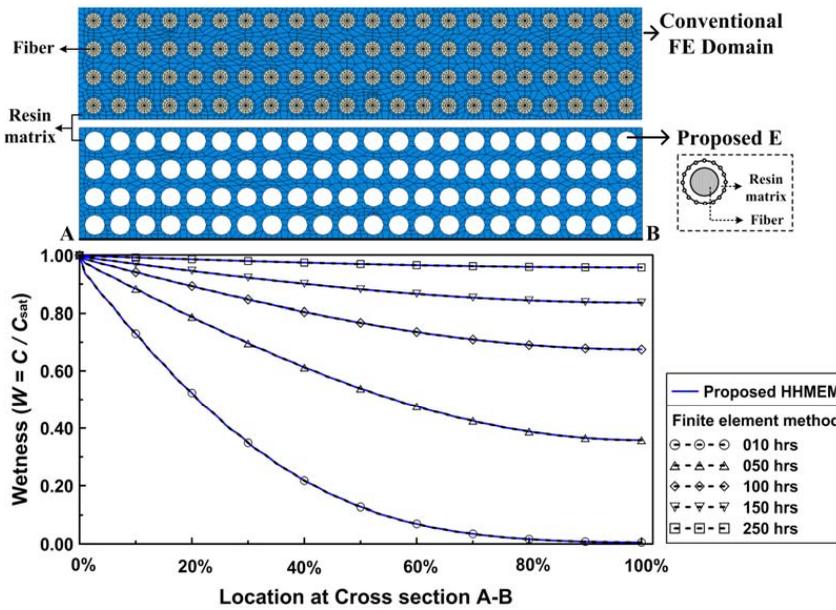| Numerical method	Total nodes	Total DOFs	Equivalent DOFs
HHME-FE	1682	1682	6962
FEM (ABAQUS)	5994	5994	5994

Figure 7: Moisture diffusion from 10th to 250th hours

4 Numerical example

Let us consider a unidirectional fiber-reinforced composite. The fibers are assumed to be straight, parallel and distributed periodically in the resin matrix. The particular geometry of the fiber permits consideration of only the cross section in the perpendicular direction of the fiber direction, reducing the analysis to a two dimensional problem as shown in Fig. 8. In examining the moisture diffusion properties of a heterogeneous composite containing multiple permeable fibers, two patterns of fiber distribution are considered in the resin matrix, square and hexagonal arrays (as shown in Fig. 9).

The composite is assumed to be heterogeneous and to have a length and width of 500μ m and 100μ m, respectively (i.e. a thickness ratio of 5:1). A moisture condition of 35ºC/85% RH is applied at the left side of the structure. Zero normal gradient conditions are used on the top, bottom and right sides of the structure. The time step increment is 180 s. The moisture related material properties of the resin matrix and permeable fibers under the applied moisture conditions of 35ºC/85% RH are presented in Tab. 2 [Laurenzi, Albrizio and Marchetti (2008)].
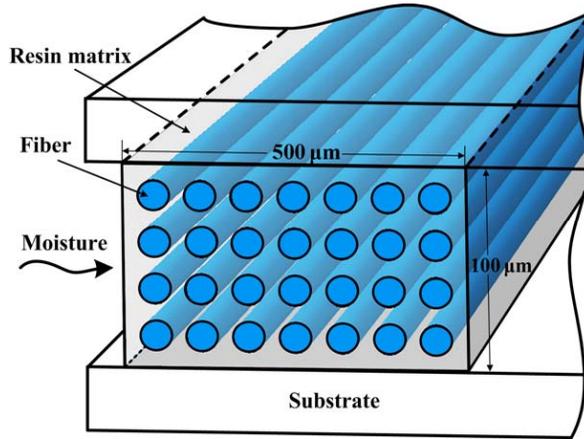
Figure 8: Schematic of a unidirectional fiber-reinforced composite

4.1 *Transient moisture diffusion process of Square and Hexagonal arrays*

The transient moisture diffusion process in the 2-D composite material with multiple fibers (inclusions) shown in Fig. 9 was analyzed using the proposed HHME-FE computational model. To represent a typical heterogeneous composite, the modeling considered two patterns of fiber distribution: square and hexagonal arrays, with a fiber volume fraction of 27% ($vf = 0.27$). The fibers were assumed to be circular with a radius of 7μ m. The radius of the HHME domain is 9μ m. Finally, the surface was exposed to a humidity of 85% RH. As previously described, in the computational model, the regions of the resin matrix occupied by the fibers were replaced by HHMEs such that only one HHME equivalent hybrid moisture capacitance/conductance matrix required calculation for each of the same HHMEs. Hence, the total number of DOFs and the PC memory storage requirements are reduced. The HHMEM parameters of the inclusion and inter-phase regions are, respectively: $\lambda = 0.5$ and $c = 0.777$; and $p = 3$ and $s = 1$. In the HHME-FE model, a total of 1056 master nodes are used, with 12 nodes on each of the 88 HHME sub-domains, and 1136 and 1126 four-node quadrilateral elements in the FE sub-domain for square and hexagonal arrays, respectively.

Using a color-scale notation, Fig. 9 illustrates the moisture distribution profiles within the fiber-reinforced composite structures at four moisture exposure times, i.e. 10th, 50th, 100th and 150th hours, respectively. In the region close to the exposed surface, it is apparent that the moisture content immediately becomes saturated, i.e. the moisture wetness variable attains a value of W = 1. In fact, this represents the boundary condition prescribed along the exposed plane. The mois-

ture is then transported progressively along the resin matrix and permeable fibers as the moisture exposure time increases.

Fig. 10 illustrates the variation in the moisture wetness of the resin matrix adjacent to the lower boundary with the elapsed exposure time. After the 250th hours, the variation of the moisture wetness along the length of the resin matrix is very small, that is, the entire resin matrix is almost fully saturated with moisture. The results of Figures 9 and 10 show that the moisture diffusion of the hexagonal array is somewhat slower than that of the square pattern under the same volume fraction of fibers at the same moisture exposure time.
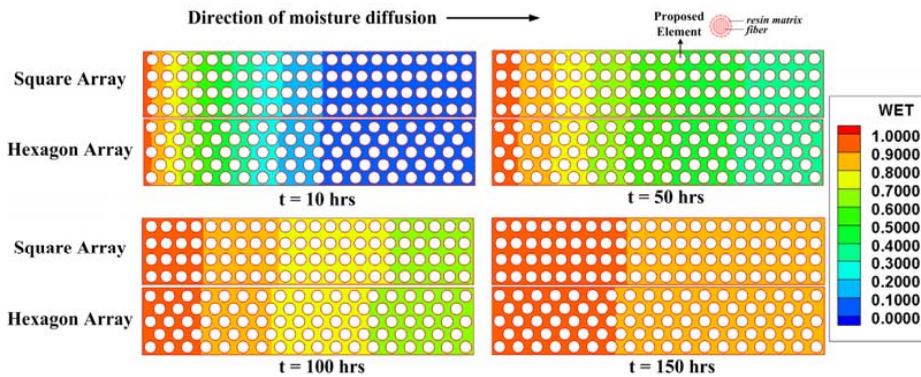

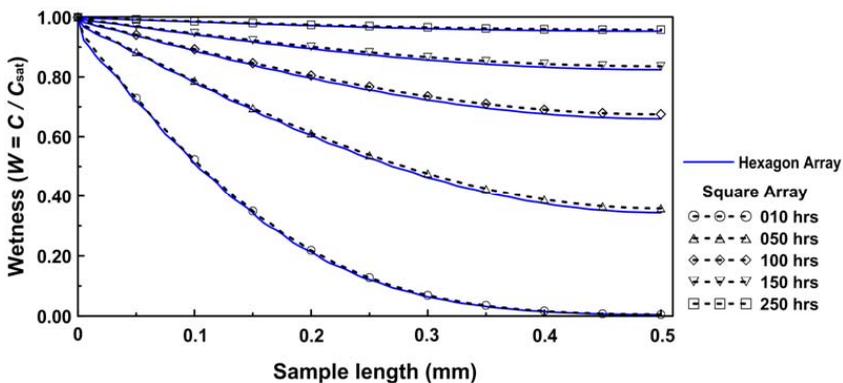Figure 9: Transient moisture distribution at varying moisture exposure times

Figure 10: Moisture diffusion in resin matrix with *vf*=0.27 from 10th to 250th hours

4.2   *Influence of volume fraction of fibers on moisture diffusion*

The coupled HHME-FE scheme was applied in order to investigate the moisture diffusion characteristics of the resin matrix containing hexagonal distributed fibers with various volume fractions, i.e. 10 to 70 percent in six equal steps, respectively. The corresponding results are presented in Fig. 11.

In the HHME sub-domain of the HHME-FE computational model, the material properties of the inter-phase region are identical to those in the matrix region (that is, the resin matrix). Therefore, the inter-phase is not modeled explicitly. Furthermore, it is assumed that a perfect bonding exists between the fibers and the resin matrix. Hence, different fiber volume fractions can be modeled without modifying the original model simply by controlling the size of the inter-phase region within the HHME domain. The HHMEM parameters of the respective inclusion and inter-phase regions are listed in Tab. 5 for each volume fraction studied. In the hexagonal fiber HHME-FE model, a total of 1056 master nodes are used, with 12 nodes on each of the 88 HHME sub-domains, and 840 four-node quadrilateral elements in the FE sub-domain.

Fig. 11 shows the effect of varying volume fractions of fibers, i.e. 10 to 70 percent in three steps, in the resin matrix adjacent to the lower boundary on moisture diffusion. The moisture which reaches the far end of the resin matrix reduces as the volume fraction of the fibers increases. The physical explanation for this is that the hexagonal distributed fibers impede moisture transfer, particularly at higher volume fractions. The result implies that a fiber-reinforced composite should be constructed using a resin matrix containing a high volume fraction of fibers in order to provide long-term durability with maximum protection against the effects of moisture penetration. Most importantly, different fiber volume fractions can be modeled without modifying the original model simply by controlling the size of the inter-phase region within the HHME domain. This advantage of the HHME approach becomes particularly apparent when the scheme is applied to investigate the relationship between the fiber volume fraction and the moisture diffusion characteristics of a heterogeneous composite material filled with multiple fibers.

5   Conclusion

This study has developed a heterogeneous hybrid moisture element method (HH-MEM) for modeling and analyzing moisture diffusion in a heterogeneous resin composite containing multiple permeable fibers. A special finite element, called heterogeneous hybrid moisture element (HHME), was proposed in order to model heterogeneous materials like imbedded inclusions with surrounding inter-phases. The heterogeneous region was subdivided into two sub-domains containing the in-

Table 5: HHMEM parameters for each studied volume fraction

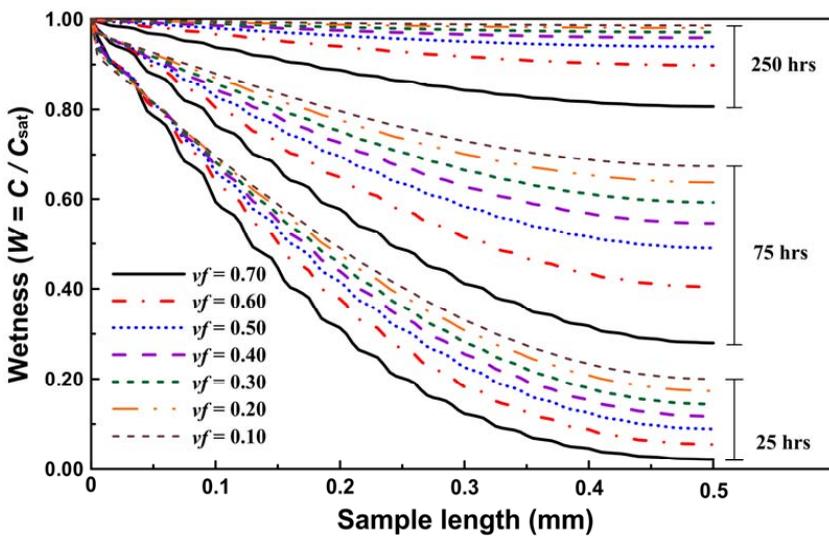| Volume fraction	Inclusion		Inter-phase	
	λ	p	c	s
10%	0.5	1	0.379	6
20%	0.5	1	0.537	5
30%	0.5	2	0.657	4
40%	0.5	3	0.759	3
50%	0.5	4	0.849	2
60%	0.5	5	0.930	1
70%	0.5	6	0	0

Figure 11: Effects of varying volume fractions of fibers in resin matrix on moisture diffusion

clusion part and the inter-phase part. The characteristic of HHME is determined by an equivalent hybrid moisture capacitance/conductance matrix. This matrix is calculated using the conventional FEM in space discretization as well as the θ-method in time discretization with similar mass/stiffness properties and matrix condensing operations. A coupled HHME-FE scheme has been developed and implemented using MATLAB language.

The performance of the proposed HHME-FE method, by comparing the results obtained for the moisture distribution profiles in a heterogeneous resin composite

with those obtained from the conventional FEM scheme, is validated. Second, the modeling approach was employed to investigate various aspects of the transient moisture diffusion process in a heterogeneous resin composite containing square and hexagonal distributed fibers. Specifically, the analysis investigated the effect of the volume fraction of fibers on the rate of moisture diffusion. The results showed that the amount of moisture penetrating the resin composite reduces significantly as the fraction volume of fibers increases. Therefore, it can be inferred that a fiber-reinforced composite should be constructed using a resin matrix with a high volume fraction of fibers in order to protect the inner components against moisture ingression.

The modeling approach proposed in this study has a number of key advantages when applied to an analysis of transient moisture diffusion in heterogeneous materials with embedded multiple inclusions. Firstly, in the computational model, the regions of the resin occupied by the fibers are all replaced by HHMEs such that only one HHME equivalent hybrid moisture capacitance/conductance matrix requires calculation for all HHMEs with the same characteristics. Hence, the execution time in the mesh modeling stage, the total number of DOFs in the computational model, and the PC memory storage and processing requirements are considerably reduced. Secondly, varying volume fractions of fibers can be modeled without modifying the original model simply by controlling the size of the inter-phase region within the HHME domain. Finally, the results obtained from the proposed method are in very good agreement with those of the conventional FEM scheme.

References

Aditya, P.K.; Sinha, P.K. (1996): Moisture diffusion in variously shaped fibre reinforced composites. *Comput. Struct.*, vol. 59, no. 1, pp. 157-166.

Browning, C.E.; Husman, G.E.; Whitney, J.M. (1977): Moisture effects in epoxy resin matrix composites. *Composite Materials: Testing and Design, ASTM STP 617*, pp. 481-496.

Crank, J.; Park, G.S. (1956): *The Mathematics of Diffusion*. Oxford University Press.

Crank, J.; Nicolson, P. (1947): A practical method for numerical evaluation of solutions of partial differential equations of the heat conduction type. *Proceedings*

of the Cambridge Philosophical Society, vol. 43, pp. 50–64.

Guo, Z.H. (1979): Similar isoparametric elements. *Sci. Bull.*, vol. 24, no. 13, pp. 577-582.

Gueribiz, D.; Rahmani, M.; Jacquemin, F.; Frèour, S.; Guillèn, R.; Loucif, K. (2009): Homogenization of moisture diffusing behavior of composite materials with impermeable or permeable fibers - Application to porous composite materials. *Journal of Composite Materials*, vol. 43, no. 12, pp. 1391-1408.

Hibbitt, D.; Karlsson, B.; Sorensen, P. (2004): *ABAQUS User's Manual Version 6.5*. Pawtucket, RI.

Kwon, Y.W.; Bang, H. (2000): *The Finite Element Method using MATLAB, second ed.* CRC Press, New York.

Laurenzi, S.; Albrizio, T.; Marchetti, M. (2008): Modeling of Moisture Diffusion in Carbon Braided Composites. *International Journal of Aerospace Engineering*, vol. 2008, article id. 294681, 10 pages.

Lewis, R.W.; Morgan, K.; Thomas, H.R.; Seetharamu, K.N. (1996): *The Finite Element Method in Heat Transfer Analysis*, Wiley, New York, pp. 81-87.

Liu, D.S.; Chiou, D.Y. (2003): A coupled IEM/FEM approach for solving the elastic problems with multiple cracks. *Int. J. Solids Struct.*, vol. 40, pp. 1973-1993.

Liu, D.S.; Chiou, D.Y. (2003): 3D IEM formulation with an IEM/FEM coupling scheme for solving elastostatic problems. *Adv. Eng. Softw.*, vol. 34, pp. 309-320.

Liu, D.S.; Chiou, D.Y. (2005): 2D infinite element modeling for elastostatic problems with geometric singularity and unbounded domain. *Comput. Struct.*, vol. 83, pp. 2086-2099

Liu, D.S.; Chiou, D.Y.; Lin C.H. (2004): A hybrid 3D thermo-elastic infinite element modeling for area-arrey package solder joints. *Finite Elem. Anal. Des.*, vol. 40, pp. 1703-1727.

Liu, D.S.; Chiou, D.Y. (2004): Modeling of inclusion with interphases in heterogeneous material using the infinite element method. *Comp. Mater. Sci.*, vol. 31, pp. 405-420.

Liu, D.S.; Chen, C.Y.; Chiou, D.Y. (2005): 3D Modeling of a composite material reinforced with multiple thickly coated particles using the infinite element method. *CMES-Comp. Model. Eng.*, vol. 9, pp. 179-191.

Pahr, D. H.; Böhm, H. J. (2008): Assessment of mixed uniform boundary conditions for predicting the mechanical behavior of elastic and inelastic discontinuously reinforced composites. *CMES: Computer Modeling in Engineering & Sciences*, vol. 34, pp. 117-136.

Shen, C.H.; Springer G.S. (1977): Moisture absorption and desorption of composite materials. *Journal of Composite Materials*, vol. 10, no. 1, pp. 2-20.

Tsai, S.W.; Hahn, H.T. (1980): *Introduction to Composite Materials*. Westport, Conn.: Technomic Pub.

Takashima, S.; Nakagaki, M.; Miyazaki, N. (2007): An elastic-plastic constitutive equation taking account of particle size and its application to a homogenized finite element analysis of a composite material. *CMES: Computer Modeling in Engineering & Sciences*, vol. 20, pp. 193-202.

Vaddadi, P.; Nakamura, T.; Singh, R.P. (2003): Inverse analysis for transient moisture diffusion through fiber reinforced composites. *Acta Mater.*, vol. 51, no. 1, pp. 177-193.

Vaddadi, P.; Nakamura, T.; Singh, R.P. (2003): Transient hygrothermal stresses in fiber reinforced composites: A heterogeneous characterization approach. *Compos. Part A*, vol. 34, no. 8, pp. 719-730.

Wong, E.H.; Teo, Y.C.; Lim, T.B. (1998): Moisture diffusion and vapor pressure modeling of IC packaging. *Proceedings of the 48th ECTC*, pp. 1372-1378.

Wong, E.H.; Rajoo, R.; Koh, S.W.; Lim, T.B. (2002): The mechanics and impact of hygroscopic swelling of polymeric materials in electronic packaging. *J. Electron. Packaging*, vol. 124, no, 2, pp. 122-126.

Yang, J.; Yang, Q.; Ma, L.; Liu, W. (2010): Moisture diffusion behavior of permeable fiber-reinforced polymer composite. *Frontiers of Mechanical Engineering in China*, vol. 5, no. 3, pp. 347-352.

Ying, L.A. (1995): *Infinite Element Methods*. Peking University Press and Vieweg Publishing.